Quantum entangled ground states of two spinor Bose-Einstein condensates

Z. F. Xu, R. Lü, and L. You

Phys. Rev. A **84**, 063634 — Published 27 December 2011

DOI: 10.1103/PhysRevA.84.063634

Quantum entangled ground states of two spinor Bose-Einstein condensates

Z. F. Xu,[1] R. Lü,[1] and L. You[1]

[1]*State Key Laboratory of Low Dimensional Quantum Physics, Department of Physics, Tsinghua University, Beijing 100084, China*

We revisit in detail the non-mean-field ground-state phase diagram for a binary mixture of spin-1 Bose-Einstein condensates including quantum fluctuations. The non-commuting terms in the spin-dependent Hamiltonian under single spatial mode approximation make it difficult to obtain exact eigenstates. Utilizing the spin z-component conservation and the total spin angular momentum conservation, we numerically derive the information of the building blocks and evaluate von Neumann entropy to quantify the ground states. The mean-field phase boundaries are found to remain largely intact, yet the ground states show fragmented and entangled behaviors within large parameter spaces of interspecies spin-exchange and singlet-pairing interactions.

PACS numbers: 03.75.Mn, 03.75.Gg

I. INTRODUCTION

Ultracold atomic quantum gases with spin degrees of freedom provide exceptionally clean and idealized testing beds for studying quantum magnetism [1, 2]. Optical trapping from ac Stark shifts of off-resonant laser fields are capable of equal confinement for all atomic pseudospin components which facilitates research into exciting spinor physics with atomic quantum gases. As is often employed in studying a trapped Bose gas, when treating the condensate, we first take a mean-field (MF) approximation assuming only one eigenvalue of the single-particle density matrix is macroscopic, being of order N. Second quantization is then limited to the condensate mode. Such a simple scenario already allows for many interesting quantum many body phenomena[3].

Two popular atomic species often employed in experimental research on spinor Bose-Einstein condensates (BECs) [3–9], are ^{87}Rb and ^{23}Na atoms. Within each species, their interactions are dominated by the density-dependent interaction in comparison to the much weaker spin-dependent interactions. As a result, single-spatial mode approximation (SMA), whereby the spatial dependence of the condensate wave function is determined independent of the spin degrees of freedom, was introduced [6] and remains reasonable as long as the number of atoms is not too large [10]. Within the MF approximation, the ground state of a spinor Bose-Einstein condensate (BEC) is found to be ferromagnetic, polar, or cyclic phases, *etc*, determined by the spin-dependent interactions and the total (hyperfine-)spin F of the atom. Further theoretical work armed with full quantum calculations reveal interesting many-body states [6, 7, 9, 11], beyond the scope of those from MF approximations. For spin-1 condensates, the exact eigenstates will contain paired spin singlets [6, 7, 11], which become more complex for higher spin condensates. For example, the spin-2 case involves spin singlets which can be formed by either two or three atoms [7, 9]. A general procedure exists for more detailed information of the building blocks of eigenstates determined by their associated generating functions [12]. More generally, we can always resort to the means of numerics to diagonalize the ground-state single-particle density matrix, which then reveals fragmented ground states if more than one eigenvalues are being of order N[13].

Several groups have recently studied spinor condensate mixtures [17–24], which also display non-MF features, such as anomalous quantum fluctuations for each spin components and quantum entangled ground states. This is first discovered in spinor condensates with more than one orbitals, for instance, the case of pseudo spin-1/2 condensates [14–16] for which Kuklov and Svistunov [14] predicted that in the ground states all atoms will have to condense into two orthogonal spatial orbitals or more due to the conservation of the total spin. This could result in a condensate ground state being a maximally entangled many-body state. Shi *et al.* replaced the two orbitals with two different atomic species, a ground state with entangled order parameter follows [16]. Under MF approximation, we have previously elaborated the ground-state phase diagram for a condensate mixture of two spin-1 BECs [18]. The interesting phases are named appropriately as FF, AA, PP, CC, and MM phases, distinguishing different structures and interaction parameter spaces. Furthermore, we provide many beyond MF results based on a full quantum spin-dependent Hamiltonian [19], which contains non-commuting terms, forbidding a simple derivation of the exact eigenstates. For two special cases, commutations are restored among the generally non-commuting terms. First, when the interspecies singlet pairing interaction is ignored ($\gamma = 0$), the Hamiltonian is then simply composed of three operators which obey the angular momentum algebra. Making use of the eigenstates of single spin-1 condensates, we directly construct the eigenstates of a binary spin-1 mixture using the angular momentum coupling representation. Second, when the interspecies anti-ferromagnetic spin-exchange interaction is strong enough, the ground state will be forced to develop entanglement between the two species [19], a result consistent with what is discovered in a spin-1 condensate placed inside a double well [25]. Other interesting features are discussed for $\gamma = 0$ revealing fragmen-

tation and quantum entanglement [20, 21, 23].

II. THE MODEL HAMILTONIAN

In this revisit we hope to understand quantum entanglement between two spin-1 condensates when both interspecies spin-exchange and singlet-pairing interactions are present. Our study is based on the same model system of a binary mixture of spin-1 condensates confined in optical traps. The corresponding field operators that annihilates a boson of species 1 and species 2 at position $\mathbf{r}$ are described respectively by $\hat{\Psi}_{M_F}(\mathbf{r})$ and $\hat{\Phi}_{M_F}(\mathbf{r})$, where $M_F = -1, 0, 1$ denoting the three Zeeman hyperfine states. The SMA is adopted for each of the two species, employing two spatial mode functions $\psi(\mathbf{r})$ and $\phi(\mathbf{r})$ respectively, and the field operators are expanded as $\hat{\Psi}_{M_F}(\mathbf{r}) = \hat{a}_{M_F}\psi(\mathbf{r})$ and $\hat{\Phi}_{M_F}(\mathbf{r}) = \hat{b}_{M_F}\phi(\mathbf{r})$, with $\hat{a}_{M_F}$ and $\hat{b}_{M_F}$ respectively the annihilation operators for an atom in the spin component M_F. In the absence of external magnetic field, the spin-dependent Hamiltonian for a binary mixture of spin-1 condensates then becomes the following

$$\begin{aligned}\hat{H}_s &= \frac{1}{2}C_1\beta_1\left(\hat{L}_1^2 - 2\hat{N}_1\right) + \frac{1}{2}C_2\beta_2(\hat{L}_2^2 - 2\hat{N}_2) \\ &+\frac{1}{2}C_{12}\beta\hat{L}_1\cdot\hat{L}_2 + \frac{1}{6}C_{12}\gamma\hat{\Theta}_{12}^\dagger\hat{\Theta}_{12}, \end{aligned} \quad (1)$$

under the SMA [19]. The interaction coefficients are $C_1 = \int d\mathbf{r}|\psi(\mathbf{r})|^4$, $C_2 = \int d\mathbf{r}|\phi(\mathbf{r})|^4$, and $C_{12} = \int d\mathbf{r}|\psi(\mathbf{r})|^2|\phi(\mathbf{r})|^2$. β_1 (β_2) is intra-species spin-exchange interaction parameter of species 1 (2). β and γ denote inter-species spin-exchange and singlet-pairing interaction parameters, respectively. The singlet pairing operator becomes $\hat{\Theta}_{12}^\dagger = \hat{a}_1^\dagger\hat{b}_{-1}^\dagger - \hat{a}_0^\dagger\hat{b}_0^\dagger + \hat{a}_{-1}^\dagger\hat{b}_1^\dagger$, and two angular momentum like operators $\hat{\mathbf{L}}_1 = \sum_{ij}\hat{a}_i^\dagger\mathbf{F}_{ij}\hat{a}_j$ and $\hat{\mathbf{L}}_2 = \sum_{ij}\hat{b}_i^\dagger\mathbf{F}_{ij}\hat{b}_j$ obey the usual angular momentum algebra [6, 26]. They commute with atom number operators $\hat{N}_1 = \sum_i\hat{a}_i^\dagger\hat{a}_i$ and $\hat{N}_2 = \sum_i\hat{b}_i^\dagger\hat{b}_i$. In the above, $\mathbf{F}_{ij}$ denotes the (i, j) component of the spin-1 matrix $\mathbf{F}$.

III. GROUND-STATE PHASE DIAGRAM

As presented in the earlier study of [19], for the spin-dependent Hamiltonian of Eq. (1), the first three terms commute with each other, but they do not commute with the fourth term. This shows the ground state determined will depend on the interaction parameters. As a result, we resorted to the special cases of no interspecies singlet-pairing interaction ($\gamma = 0$) and $C_1\beta_1 = C_2\beta_2 = C_{12}\beta/2$ [19]. For the first case of $\gamma = 0$, it has already attracted much attention due to the appearance of fragmented ground states and the associated entanglement between two species and exotic atomic number fluctuations [19–21].

In this study, we will discuss the general case of the full spin-dependent Hamiltonian of Eq. (1). Whenever the ground state depends on the interaction parameters, we have to perform a full quantum calculation numerically, usually this amounts to a full exact numerical diagonalization for each atom numbers N_1 and N_2. Before discussing the numerical results, we want to point out that there still exist two conserved quantities: the total spin angular momentum and its z-component, as $\hat{L}^2 = (\hat{L}_1 + \hat{L}_2)^2$ commutes with the spin-dependent Hamiltonian. As a result, we can elaborate spin structures from building blocks derived by generating function of the maximum spin states $|l, l_z = l\rangle$, where we have used quantum numbers l and l_z to denote the common eigenstates of the angular momentum operators $\hat{L}^2$ and $\hat{L}_z$.

We recall the suitable generating function $G_g(x, y, z)$ for a binary mixture of two spin-1 condensates derived earlier in Ref. [19]. From this generating function, we have figured out all six building blocks for constructing the eigenstate $|l, l\rangle$, which is given by

$$\begin{aligned}|l,l\rangle = \sum \mathcal{C}(\{u_i\},\{v_i\},\{w_i\})\big(\hat{A}_1^{(1)\dagger}\big)^{u_1}\big(\hat{A}_0^{(2)\dagger}\big)^{u_2}\big(\hat{B}_1^{(1)\dagger}\big)^{v_1} \\ \times\big(\hat{B}_0^{(2)\dagger}\big)^{v_2}\big(\hat{\Gamma}_0^{(1,1)\dagger}\big)^{w_1}\big(\hat{\Gamma}_1^{(1,1)\dagger}\big)^{w_2}|\text{vac}\rangle, \end{aligned} \quad (2)$$

where the six building blocks are

$$\begin{aligned}\hat{A}_1^{(1)\dagger} &= \hat{a}_1^\dagger, \\ \hat{A}_0^{(2)\dagger} &= \hat{a}_0^{\dagger 2} - 2\hat{a}_1^\dagger\hat{a}_{-1}^\dagger, \\ \hat{B}_1^{(1)\dagger} &= \hat{b}_1^\dagger, \\ \hat{B}_0^{(2)\dagger} &= \hat{b}_0^{\dagger 2} - 2\hat{b}_1^\dagger\hat{b}_{-1}^\dagger, \\ \hat{\Gamma}_0^{(1,1)\dagger} &= \hat{\Theta}_{12}^\dagger, \\ \hat{\Gamma}_1^{(1,1)\dagger} &= \frac{1}{\sqrt{2}}\left(\hat{a}_1^\dagger\hat{b}_0^\dagger - \hat{a}_0^\dagger\hat{b}_1^\dagger\right), \end{aligned} \quad (3)$$

and u_i ,v_i, and w_i satisfy the constrains

$$\begin{aligned}u_1 + 2u_2 + w_1 + w_2 &= N_1, \\ v_1 + 2v_2 + w_1 + w_2 &= N_2, \\ u_1 + v_1 + w_2 &= l, \end{aligned} \quad (4)$$

and additionally $w_2 = 0, 1$. Spin states $|l, l_z \neq l\rangle$ of other magnetization can be constructed by simply applying $(\hat{L}_-^{l-l_z}$ on the state $|l, l\rangle$ as $\hat{L}_-^{l-l_z}|l, l\rangle \propto |l, l_z \neq l\rangle$ (un-normalized).

In most numerical studies, we assume each species contain 100 atoms ($N_1 = N_2 = N = 100$). Due to the SO(3) symmetry of our model, we restrict the Hilbert space into the subspace of zero magnetization with $l_z = 0$ [27]. In Fig. 1, we summarize the extensive numerical results. Since the total spin angular momentum is conserved, we can use the eigenvalue of the operator $\hat{L}^2$ to distinguish different phase, which is then accompanied by the information of the building blocks. A total of three constrains exist for the allowed values of u_i, v_i, and w_i ($i = 1, 2$). Only three are needed for a solution, we choose the three

as u_2, v_2 and w_1, which are determined numerically from evaluating the associated expectation values of $\hat{A}_0^{(2)\dagger}\hat{A}_0^{(2)}$, $\hat{B}_0^{(2)\dagger}\hat{B}_0^{(2)}$, and $\hat{\Gamma}_0^{(1,1)\dagger}\hat{\Gamma}_0^{(1,1)}$, respectively.

From extensive numerical results we construct the ground-state phase diagram as shown in Fig. 1. Perhaps not surprisingly, it is almost the same as the MF approximation studied in Ref. [18]. Each phase is then labeled the same as before [18], albeit that the meanings can be different due to the non-commuting operators in the spin-dependent Hamiltonian Eq. (1). In Tab. I, we summarize the properties for the four special phases: FF, AA, PP, and CC. The remaining MM phase still denotes the phase whose parameters evolve continuously across the phase boundaries.

	$\langle\hat{L}^2\rangle$	$\langle\hat{A}_0^{(2)\dagger}\hat{A}_0^{(2)}\rangle$	$\langle\hat{B}_0^{(2)\dagger}\hat{B}_0^{(2)}\rangle$	$\langle\hat{\Gamma}_0^{(1,1)\dagger}\hat{\Gamma}_0^{(1,1)}\rangle$
FF	$=2N(2N+1)$	$=0$	$=0$	$=0$
AA	$=0$	~ 0	~ 0	$\sim N(N+2)$
PP	$=0$	$\sim N(N+1)$	$\sim N(N+1)$	~ 0
CC1	$=N(N+1)$	$\sim N(N+1)$	~ 0	$\sim N(N+2)$
CC2	$=0$	$\sim N(N+1)$	$\sim N(N+1)$	$\sim N(N+2)$
CC3	$=N(N+1)$	~ 0	$\sim N(N+1)$	$\sim N(N+2)$

TABLE I: The expectation values for the special operators in the ground state within different phases.

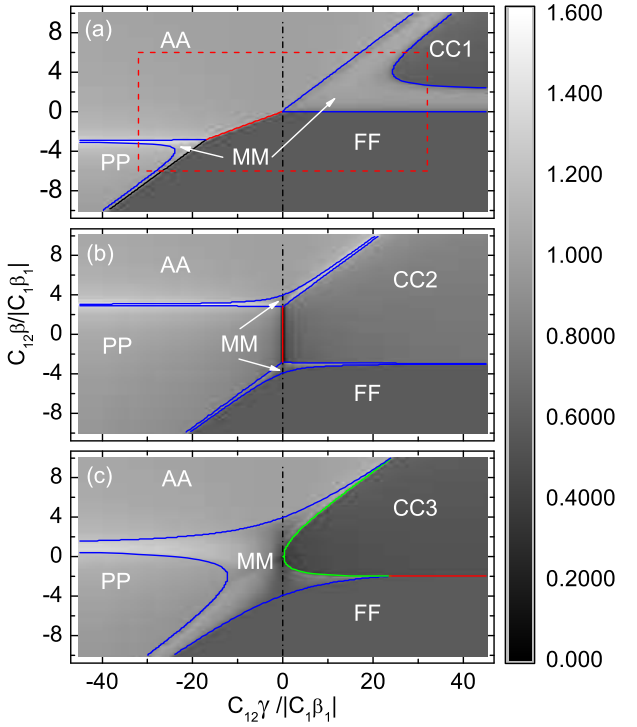

FIG. 1: (Color online). The ground-state phase diagram and the corresponding von Neumann entropy distribution at fixed values of $C_1\beta_1$ and $C_2\beta_2$. Blue solid lines denote continuous phase transition boundaries. Red solid lines denote discontinuous phase transition boundaries between two phases with fully determined total spin angular momentum l. The green solid line denotes the discontinuous phase transition boundary between the phase CC3 and the MM phase. The black dash-dotted lines correspond to $C_{12}\gamma = 0$, which serve as guides for the eye. The von Neumann entropy of the ground states are painted by gray scale density plots, where black (white) color refer to low (high) entanglement respectively. The three subplots denote fixed intra-specie spin exchange interaction parameters of $(C_1\beta_1, C_2\beta_2)/|C_1\beta_1| =:$ (a) $(-1,-2)$; (b) $(1,2)$; and (c) $(-1,2)$. The red dashed lines are four lines connecting the points $O_{\rm AA}(-32,6)$, $O_{\rm CC}(32,6)$, $O_{\rm FF}(32,-6)$ and $O_{\rm PP}(-32,-6)$ in the parameter space of $(C_{12}\gamma, C_{12}\beta)/|C_1\beta_1|$.

IV. ENTANGLED GROUND STATES

To quantify entanglement between the two species, we numerically computed the von Neumann entropy $S(\hat{\rho}_1) = -\mathrm{Tr}(\hat{\rho}_1 \log_{2N+1}\hat{\rho}_1)$, where $\hat{\rho}_1 = \mathrm{Tr}_2\hat{\rho}$ is the reduced density matrix resulting from partial tracing of the ground-state density matrix $\hat{\rho}$ over the basis of species 2. The amount of entanglement is then shown as density plots over the phase diagram of Fig. 1, with a legend shown on the right, the black (white) color refer to low (high) entanglement.

In the absence of interspecies singlet-pairing interaction ($\gamma = 0$), the spin-dependent Hamiltonian of Eq. (1) contains only three operators commuting with each other. As a result we can use quantum numbers l_1, l_2, l, and l_z to quantify its eigenstate $|l_1, l_2, l, l_z\rangle$, with $\langle\hat{L}_1^2\rangle = l_1(l_1+1)$, $\langle\hat{L}_2^2\rangle = l_2(l_2+1)$, $\langle\hat{L}^2\rangle = l(l+1)$ and $\langle\hat{L}_z\rangle = l_z$. In the ground states, we have $l = l_1 + l_2$ for ferromagnetic interspecies spin-exchange interaction ($\beta < 0$); and $l = |l_1 - l_2|$ for anti-ferromagnetic interspecies spin-exchange interaction ($\beta > 0$), while the value of l_1 and l_2 are determined by the three interaction parameters.

In Fig. 2, we display the expectation values of the intra- and interspecies single-pairing number operators in the ground state, divided by their corresponding maximum values shown in Tab. I. In addition, we show the total spin angular momentum and the von Neumann entropy. First, when $(\beta_1 < 0, \beta_2 < 0)$, irrespective of the interspecies spin-exchange interaction, atoms in the same species will not pair into a singlet, but atoms in different species will pair into singlets with $\langle\Gamma_0^{(1,1)\dagger}\Gamma_0^{(1,1)}\rangle$ close to reaching its maximum values $N(N+2)$ when the interspecies spin-exchange interaction is anti-ferromagnetic. The corresponding total spin angular momentum $\hat{L}^2$ is equal to its maximum value $2N(2N+1)$ with a relatively low von Neumann entropy when the interspecies spin-exchange interaction is ferromagnetic. The total spin angular momentum $\hat{L}^2$ is equal to 0 with the von Neumann entropy $S(\hat{\rho}_1) = 1$ for anti-ferromagnetic interspecies spin-exchange interaction. Second, when $(\beta_1 > 0, \beta_2 > 0)$, in the two limits of large ferromagnetic or anti-ferromagnetic interspecies spin-exchange interaction, the ground state is the same as above in the previous case. In the other limit with low interspecies spin-exchange interaction, atoms in the same species tend to pair into

singlets giving rise to no entanglement between the two species. This implies the ground state can be written as a product state: $Z^{-1/2}(\hat{A}_0^{(2)\dagger})^{N/2}(\hat{B}_0^{(2)\dagger})^{N/2}|\text{vac}\rangle$. For the remaining phase, we call it the MM phase, which can show higher (lower) entanglement compared to the FF phase between the two species when $\beta > 0$ ($\beta < 0$). For the final case when $(\beta_1 < 0, \beta_2 > 0)$, the ground state show similar properties as that in the second case.

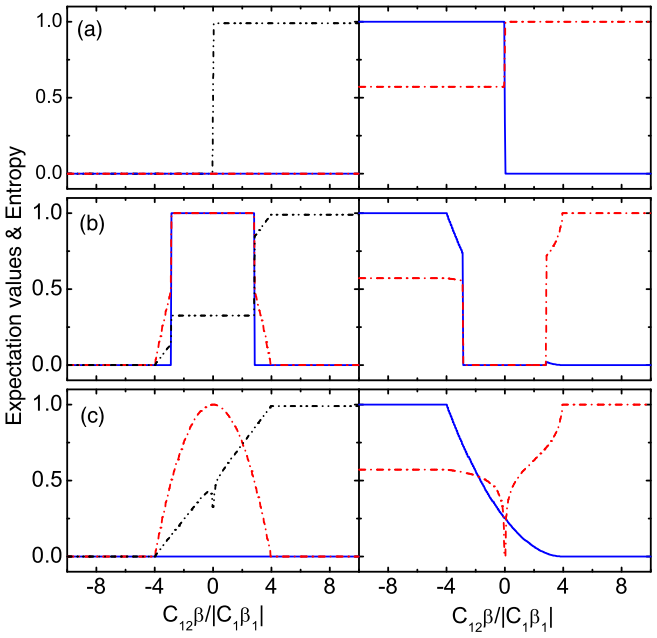

FIG. 2: (Color online). LEFT: The ground-state normalized expectation values of intra- and interspecies singlet-pairing number operators $\hat{A}_0^{(2)\dagger}\hat{A}_0^{(2)}/N(N+1)$, $\hat{B}_0^{(2)\dagger}\hat{B}_0^{(2)}/N(N+1)$, $\hat{\Gamma}_0^{(1,1)\dagger}\hat{\Gamma}_0^{(1,1)}/N(N+2)$, denoted by blue solid, red dash-dot, and black dash-dot-dot lines, respectively. RIGHT: The normalized total spin angular momentum $\hat{L}^2/2N(2N+1)$ and von Neumann entropy of the ground state, denoted by blue solid and red dash-dot lines, respectively. The three subplots denote zero interspecies singlet-pairing interaction ($\gamma = 0$) and fixed intra-species spin-exchange interaction parameters $(C_1\beta_1, C_2\beta_2)/|C_1\beta_1|$ =: (a) $(-1,-2)$; (b) $(1,2)$; and (c) $(-1,2)$.

The most attractive phase when $\gamma = 0$ is the entangled ground state denoted by ψ_{AA}^{00} [19],

$$\psi_{\text{AA}}^{00} = \frac{1}{\sqrt{2N+1}} \sum_{m=-N}^{N} (-)^{N-m}|N,m\rangle_1 \otimes |N,-m\rangle_2, \quad (5)$$

which show high entanglement with $S(\hat{\rho}_1) = 1$ between the two species. As demonstrated in Fig. 1 by numerical calculations, however, there remain other phases which show larger entanglement between the two species. This shows that the state ψ_{AA}^{00} is not a maximal entangled state, in contrast to previously studied case of two pseudo spin-1/2 condensates [16]. This is not a surprise [28]. Due to the redundant degrees of freedom in the spin-1 case, the total spin angular momentum of each species can take other values besides the largest value of N. To demonstrate the entanglement between the two species, we show their corresponding expectation values and von Neumann entropy along four lines connecting the points $O_{\text{AA}}(-32,6)$, $O_{\text{CC}}(32,6)$, $O_{\text{FF}}(32,-6)$ and $O_{\text{PP}}(-32,-6)$ in the parameter space of $(C_{12}\gamma, C_{12}\beta)/|C_1\beta_1|$. The four lines are marked as red dashed lines in the Fig. 1(a).

In Fig. 3, we illustrate the ground-state properties of two ferromagnetic condensates with intraspecies spin-exchange interactions at $(C_1\beta_1, C_2\beta_2)/|C_1\beta_1| = (-1,-2)$. First of all, we consider the AA phase. When $\gamma = 0$, the spin-dependent Hamiltonian contains three operators commuting with each other, and the ground state can be expressed as ψ_{AA}^{00} for large enough antiferromagnetic interspecies spin-exchange interaction, and show high entanglement between the two species. When $\gamma \neq 0$, although the fourth term of the spin-dependent Hamiltonian does not commute with the other three, we find that the ground state not only show similar expectation values of the operators, it also contain similar entanglement between the two species, over a large area in the phase diagram demonstrated in Fig. 1(a). For $\gamma < 0$, irrespective of its value, the ground state falls into the AA phase. For $\gamma > 0$, the ground state is still classified as the AA phase, as long as $C_{12}\gamma$ does not exceed a critical value, which increases in proportion to the interspecies spin-exchange interaction parameter $C_{12}\beta$. In the first column of Fig. 3, we evaluate the properties of the AA phase, where the ground-state expectation value of intra- and interspecies singlet-pairing number operators are close to 0, 0, and $N(N+2)$, respectively. The total spin angular momentum is exactly equal to 0, and the von Neumann entropy is close to 1.

When interspecies singlet-pairing interaction exceeds a critical value, the ground state changes into the MM phase. As long as $C_{12}\gamma > 0$, it tries to decrease the interspecies singlet-pairing interaction. In the first column of Fig. 3, we follow the line of $O_{\text{AA}}O_{\text{CC}}$ and illustrate the phase transition from the AA phase into the MM phase. In the MM phase, as long as we increase $C_{12}\gamma$ accordingly, atoms in different species will continuously avoid to pair into singlets, while atoms in species 1 will try to pair into singlets. Atoms in species 2 first try to pair into singlets and then avoid to pair. Meanwhile, the total spin angular momentum first increases and then decreases. For a relatively large area of the MM phase, we find the two species show high entanglement compared to the AA phase.

As interspecies singlet-pairing interaction is increased, the ground state will fall into the CC1 phase, where its total spin angular momentum $\hat{L}^2$ will be equal to $N(N+1)$, and atoms in the species 1 (2) will pair (not pair) into singlets. At the same time the expectation value of $\Gamma_0^{(1,1)\dagger}\Gamma_0^{(1,1)}$ will be near to its maximum $N(N+2)$. The ground-state von Neumann entropy in the CC1 phase remains at a low value.

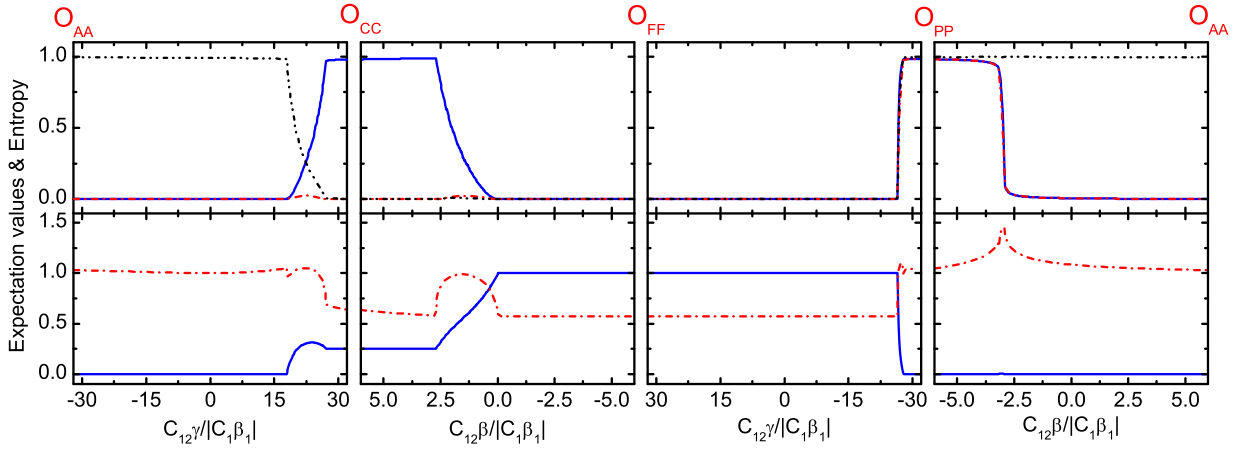

FIG. 3: (Color online). TOP: The ground-state normalized expectation values of intra- and interspecies singlet-pairing number operators $\hat{A}_0^{(2)\dagger}\hat{A}_0^{(2)}/N(N+1)$, $\hat{B}_0^{(2)\dagger}\hat{B}_0^{(2)}/N(N+1)$, $\hat{\Gamma}_0^{(1,1)\dagger}\hat{\Gamma}_0^{(1,1)}/N(N+2)$, denoted by blue solid, red dash-dot, and black dash-dot-dot lines, respectively. BOTTOM: The normalized total spin angular momentum $\hat{L}^2/2N(2N+1)$ and Von Neumann entropy of the ground state, denoted by blue solid and red dash-dot lines, respectively. From left to right, we illustrate the corresponding expectation values and Von Neumann entropy along four direct lines connecting four points $O_{\rm AA}(-32,6)$, $O_{\rm CC}(32,6)$, $O_{\rm FF}(32,-6)$ and $O_{\rm PP}(-32,-6)$ in the parameter space of $(C_{12}\beta, C_{12}\gamma)/|C_1\beta_1|$. The intraspecies spin-exchange interactions are fixed at $(C_1\beta_1, C_2\beta_2)/|C_1\beta_1| = (-1,-2)$. The four lines are marked as red dashed lines in the Fig. 1(a).

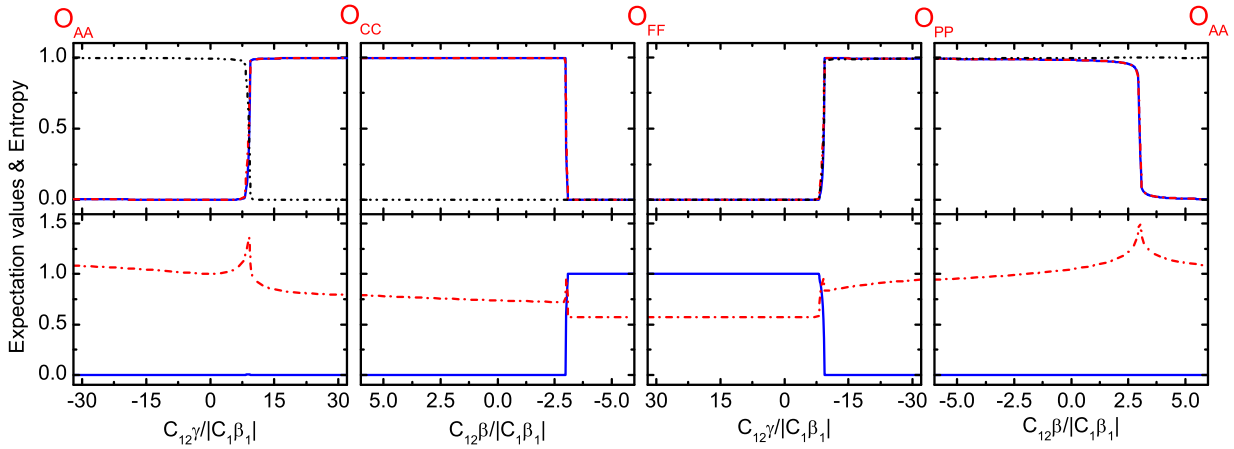

FIG. 4: (Color online). The same as that in Fig. 3, but with different intraspecies spin-exchange interactions fixed at $(C_1\beta_1, C_2\beta_2)/|C_1\beta_1| = (1,2)$.

Going along the line $O_{\rm CC}O_{\rm FF}$, with decreasing interspecies spin-exchange interaction, the ground state changes from the CC1 phase, to the MM phase, and finally to the FF phase. Atoms of species 1 will become unpaired continuously, while the total spin angular momentum increases from $N(N+1)$ in the CC1 phase to its maximum $2N(2N+1)$ in the FF phase. The ground-state entanglement between the two species in the CC1 and the FF phase are almost at the same level. While in the MM phase, the entropy first increases to near 1 and then decreases.

We then follow the line $O_{\rm FF}O_{\rm PP}$. With decreasing interspecies singlet-pairing interaction, the ground state covers the FF, MM, and PP phases successively. In the PP phase, atoms in the same/different species will all try to pair into singlets. The ground-state expectations values for intra- and interspecies singlet-pairing number operators will reach close to their corresponding maximum, meanwhile the two species show higher entanglement. In the MM phase, the expectations values for operators or the von Neumann entropy change continuously to connect the FF phase and the PP phase.

Lastly, we consider the line $O_{\rm PP}O_{\rm AA}$. As long as the interspecies spin-exchange interaction increases, the ground state will be changed continuously from the PP to the MM, and to the AA phase. From the fourth column of Fig. 3, we find that in the whole line of $O_{\rm PP}O_{\rm AA}$, the two species show a relatively high entanglement with the von Neumann entropy $S(\hat{\rho}_1)$ remaining higher than 1. Especially so in the MM phase, where the highest

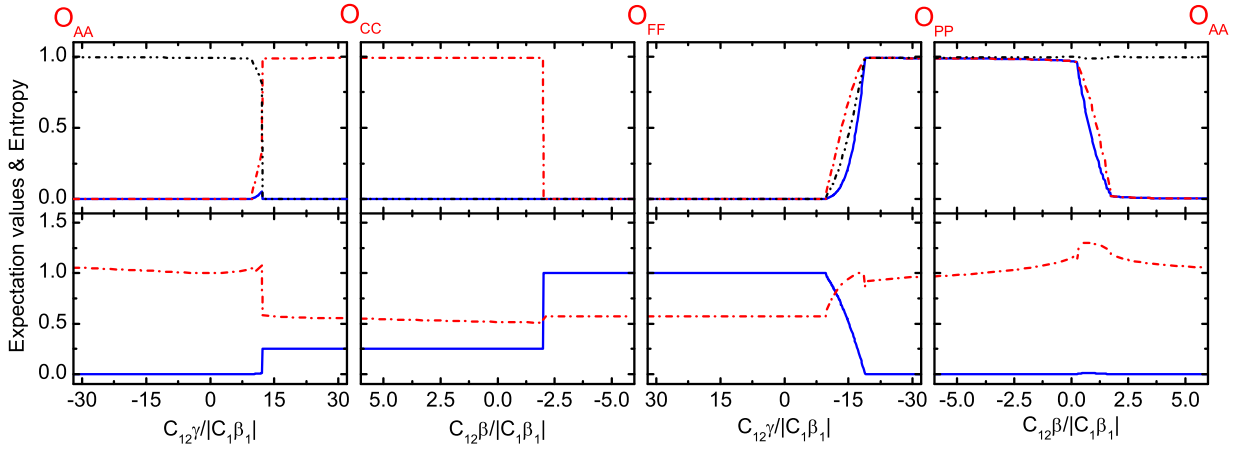

FIG. 5: (Color online). The same as that in Fig. 3, but with different intraspecies spin-exchange interactions, which are fixed at $(C_1\beta_1, C_2\beta_2)/|C_1\beta_1| = (-1, 2)$.

entropy reaches 1.4568, which is close to the maximum entropy of $\log_{2N+1}((N+1)(N+2)/2) \simeq 1.6116$.

In Figs. 4 and 5, we illustrate the two other cases with intraspecies spin-exchange interactions $(C_1\beta_1, C_2\beta_2)/|C_1\beta_1|$ fixed respectively at $(1, 2)$ and $(-1, 2)$. We find that the ground-state show similar properties to that in the two ferromagnetic condensates shown in Fig. 3. The only difference is for the CC2 or CC3 phase. In the CC2 phase, the ground state expectation values for both intra- and interspecies singlet-pairing number operators are close to their corresponding maximum $N(N+1)$, $N(N+1)$, and $N(N+2)$. While in the CC3 phase, they are close to 0, $N(N+1)$, and $N(N+2)$, respectively. The total spin angular momentum of the ground state is equal to 0 in the CC2 phase, and $N(N+1)$ in the CC3 phase. Meanwhile, in the CC2 phase the von Neumann entropy is less than 1 but larger than that in the FF phase, while in the CC3 phase, it is close to the value in the FF phase.

Before conclusion, we hope to stress that the maximal entangled state in this system is given by

$$\psi_{\rm ME} = Z^{-1/2} \left(\hat{\Gamma}_0^{(1,1)\dagger}\right)^N |{\rm vac}\rangle. \qquad (6)$$

It is the eigenstate or the ground state (if $\gamma < 0$) of the γ-term in the Hamiltonian of the Eq. (1), which means the maximal entangled state $\psi_{\rm ME}$ is the eigenstate of two spin-1 condensates with only interspecies spin-singlet pairing interaction ($\beta_1 = \beta_2 = \beta = 0$ and $\gamma \neq 0$), with the corresponding eigenvalue $C_{12}\gamma N(N+2)/6$ [29].

V. CONCLUSION

In conclusion, we have studied the ground-state phase diagram for a binary mixture of two spin-1 condensates more carefully, going beyond the MF approximation. When there exists no interspecies singlet-pairing interaction, the spin-dependent Hamiltonian contains three operators commuting with each other. In this special case, the most interesting phase is the AA phase, where two species show high entanglement. When interspecies singlet-pairing interaction is turned on, the added operators do not commute with the previous three ones, which forbids us from obtaining exact eigenstates analytically for the model spin system. In this study, we perform full quantum diagonalization to find the ground states numerically. To quantify the ground states, we work out the building blocks to construct the maximum spin states, which can be used rightfully to discuss entanglement scales between the two species. We have evaluated the associated ground-state von Neumann entropy. After detail calculations, we find that the AA phase can persist for large areas of the parameter space for interspecies spin-exchange and singlet-pairing interactions. In addition, there is another interesting phase: the PP phase, which show similar level of entanglement between the two species. What's more, we find that AA phase is not the maximum entangled state. The ground state with highest entanglement we found lies in the MM phase.

VI. ACKNOWLEDGMENTS

This work is supported by NSF of China under Grants No. 11004116, No. 10974112 and No. 91121005 , NKBRSF of China, and the research program 2010THZO of Tsinghua University.

[1] S. Trotzky, P. Cheinet, S. Fölling, M. Feld, U. Schnorrberger, A. M. Rey, A. Polkovnikov, E. A. Demler, M. D. Lukin and I. Bloch, Science **319**, 295 (2008); Maciej Lewenstein and Anna Sanpera, Science **319**, 292 (2008);

[2] David M. Weld and Wolfgang Ketterle, Journal of Physics: Conference Series **264**, 012017 (2011)

[3] Masahito Ueda and Yuki kawaguchi, arXiv:1001.2072.

[4] Tin-Lun Ho, Phys. Rev. Lett. **81**, 742 (1998).

[5] T. Ohmi and K. Machida, J. Phys. Soc. Jpn. **67**, 1822 (1998).

[6] C. K. Law, H. Pu, and N. P. Bigelow, Phys. Rev. Lett. **81**, 5257 (1998).

[7] Masato Koashi and Masahito Ueda, Phys. Rev. Lett. **84**, 1066 (2000).

[8] C. V. Ciobanu, S.-K.Yip, and Tin-Lun Ho, Phys. Rev. A **61**, 033607 (2000).

[9] M. Ueda and M. Koashi, Phys. Rev. A **65**, 063602 (2002).

[10] S. Yi, Ö. E. Müstecaplıoğlu, C. P. Sun, and L. You, Phys. Rev. A **66**, 011601 (2002).

[11] Tin-Lun Ho and Sung Kit Yip, Phys.Rev.Lett. **84**, 4031 (2000).

[12] Tin-Lun Ho and Lan Yin, Phys. Rev. Lett. **84**, 2302 (2000).

[13] Erich J. Mueller, Tin-Lun Ho, Masahito Ueda, and Gordon Baym, Phys. Rev. A **74**, 033612 (2006).

[14] A. B. Kuklov and B. V. Svistunov, Phys. Rev. Lett. **89**, 170403 (2002).

[15] S. Ashhab and A. J. Leggett, Phys. Rev. A **68**, 063612 (2003).

[16] Yu Shi and Qian Niu, Phys. Rev. Lett. **96**, 140401 (2006).

[17] Ma Luo, Zhibing Li, and Chengguang Bao, Phys. Rev. A **75**, 043609 (2007).

[18] Z. F. Xu, Yunbo Zhang, and L. You, Phys. Rev. A **79**, 023613 (2009).

[19] Z. F. Xu, Jie Zhang, Yunbo Zhang, and L. You, Phys. Rev. A **81**, 033603 (2010).

[20] Jie Zhang, Z. F. Xu, L. You, and Yunbo Zhang, Phys, Rev. A **82**, 013625 (2010).

[21] Yu Shi, Phys. Rev. A **82**, 023603 (2010).

[22] Z. F. Xu, J. W. Mei, R. Lü, and L. You, Phys. Rev. A **82**, 053626 (2010).

[23] Yu Shi and Li Ge, Phys. Rev. A **83**, 013616 (2011).

[24] Jie Zhang, Tiantian Li, and Yunbo Zhang, Phys. Rev. A **83**, 023614 (2011).

[25] Michael W. Jack and Makoto Yamashita, Phys. Rev. A **71**, 033619 (2005).

[26] Ying Wu, Phys. Rev. A **54**, 4534 (1996).

[27] The total Hilbert space for zero magnetization $l_z = 0$ of the case of $N_1 = N_2 = 100$ is 174301. Here we use ARPACK pakage to do numerical diagonalization.

[28] Ö. E. Müstecaplıoğlu, M. Zhang, and L. You, Phys. Rev. A **66**, 033611 (2002).

[29] We have previously miscalculated the operator $\hat{\mathcal{S}}_z$, which is equal to $(\hat{N}_1 + \hat{N}_2 + 3)/2$ not $(\hat{N}_1 + \hat{N}_2)/2 + 3$ in the Ref. [19]. As a result, $\mathcal{S} = (n_0 + 3)/2$ $(n_0 = 0, 1, 2, \dots)$, $\min(\mathcal{S}) = 3/2$ and $\min(\mathcal{S}_z) = 3/2$. Also the Eq. (13) in the Ref. [19] need to be changed to $E = \frac{1}{4}C_{12}\beta\, l(l+1) + \frac{1}{6}C_{12}\gamma\, n_s(n_s + n_0 + 2) - \frac{1}{2}C_{12}\beta(N^{(1)} + N^{(2)})$.